Energy 112 (2016) 43–51

Contents lists available at ScienceDirect

Energy

journal homepage: www.elsevier.com/locate/energy

# Performance analysis of a thermally regenerative electrochemical refrigerator

Baode Li, Rui Long**, Zhichun Liu, Wei Liu*

*School of Energy and Power Engineering, Huazhong University of Science and Technology, Wuhan 430074, China*

ARTICLE INFO

*Article history:*
Received 9 October 2015
Received in revised form
27 March 2016
Accepted 7 June 2016
Available online 17 June 2016

*Keywords:*
Thermally regenerative electrochemical refrigerator (TRER)
Performance analysis
Coefficient of performance (COP)
Heat leakage
Finite time thermodynamics

ABSTRACT

Performance analysis and optimization of a thermally regenerative electrochemical refrigerator (TRER) are investigated based on finite time analysis. The general expressions of some important parameters of TRER are derived. The $\chi$ figure of merit considers both the coefficient of performance (COP) and cooling load rate, which can be seen as a compromise between maximum cooling load rate and maximum COP. Based on this, the traditional region between both can be divided into two more specific performance regions that represent two different operating demands. Under the maximum $\chi$ figure of merit, the impacts of the cell material's characteristics, heat conductance of heat exchangers, and heat reservoir temperature ratio on the corresponding cooling load rate and COP are analyzed in detail. Results reveal that materials with larger isothermal coefficient, specific charging/discharging capacity, lower internal resistance, and specific heat correspond to higher cooling load rate and extracted COP. Better heat exchange performance of the regenerator increases cooling load rate and power input; however, it does not guarantee a higher corresponding COP. We expect this work to contribute to designing and operating high performance TRER devices.



## 1. Introduction

Most energy consumption originates from the combustion of fossil fuels, which are utilized through thermodynamic processes and cycles. Approximately 15% of all the electricity produced worldwide involves the use of refrigeration (air conditioning, freezing, refrigeration, etc.) [1]. Performance limits for thermodynamic processes and optimization of thermodynamic cycles have been widely studied. The traditional technology of vapor-compression refrigeration usually employs polluting or toxic refrigerants, such as chlorofluorocarbons (CFCs), that contribute to ozone depletion and greenhouse effects [2]. Therefore, exploring alternative technologies for cooling has drawn increasing attention, such as adsorption refrigeration [3], thermoelectric cooling [4], magnetic refrigeration [5], and electrochemical refrigeration [6,7].

In the past decades, alternative technologies have been proposed for thermal energy harvesting [8,9], a thermally regenerative electrochemical cycle (TREC) based on the thermogalvanic effect and temperature dependence of electrode potential has been constructed: discharging a battery at temperature $T_H$ and charging back at temperature $T_L$ [10]. Net energy is produced through the voltage difference between charging and discharging processes, and heat is absorbed at higher temperature in the meantime. In practice, TREC is a Stirling-like cycle. Regenerators have been adopted to enhance efficiency, which shows 40–50% of the Carnot limit for high-temperature application [11]. Lee et al. [12] conducted an experiment on an electrochemical system for efficient and low-cost thermal energy-harvesting, and found that heat-to-electricity conversion efficiency reaches 5.7% when cycled between 10 °C and 60 °C.Yang et al. [13] investigated a charging-free TREC system, where the two electrochemical processes at both low and high temperatures in a cycle are discharging. In addition, a membrane-free battery for TREC has been also proposed [14]. Furthermore, Long et al. [15] analyzed the impacts of cell material and heat exchangers on maximum power extracted and its corresponding efficiency of TREC for harvesting waste heat based on finite time analysis. Multi-objective optimization of a continuous TREC for waste heat recovery has been also conducted [16]. Furthermore, Long et al. [17] adopted the TREC to harvest waste heat from the proton exchange membrane fuel cell (PEMFC), and

* Corresponding author.
** Corresponding author.
*E-mail addresses:* r_long@hust.edu.cn (R. Long), w_liu@hust.edu.cn (W. Liu).

http://dx.doi.org/10.1016/j.energy.2016.06.045
0360-5442/

found that the power output of the hybrid system is 6.85%–20.59% larger than that of the PEMFC subsystem, and the total electrical efficiency is improved by 2.74%–8.27%.The efficiency of a TREC is limited by the heat capacity of materials and effectiveness of heat exchangers.

The thermally regenerative electrochemical refrigerator (TRER), which is a reverse cycle of the TREC, has also attracted increased attention [6,7,10]. The TRER system consists of two cells: a hot cell in contact with hot reservoir (usually the environment), and a cold cell in contact with cold reservoir (such as the cooling space). Both cells, where the electrochemical reactions occur, also function as heat exchangers. The cold cell consumes electricity and absorbs heat, whereas the hot cell rejects the heat and generates electricity. After a cycle, the two cells return to their initial state, and meanwhile, additional electricity should be supplied. Compared with vapor-compression refrigeration, the TRER system does not involve any moving parts and no noise is produced in the operation process.

Many studies on the performance analysis and optimization of the refrigerators have been performed based on various optimization criteria, such as power input, cooling load rate, coefficient of performance (COP), exergy output rate, exergetic efficiency, and entropy generation rate [18–23]. However, for refrigerators, the minimum power input criterion is not an appropriate optimization criterion [24]. Much effort has been dedicated to optimizing refrigerators under different figure of merits. Velasco et al. [25] obtained the upper bound of COP, i.e., the CA coefficient of performance, for endoreversible refrigerators. Jiménez de Cisneros et al. [26] investigated COP at maximum COP criterion based on the linear irreversible model. Angulo-Brown et al. [27] proposed an ecological optimization criterion, $E = P - T_L\sigma$, for finite-time Carnot heat engine, where $P$ is the power output, $T_L$ is the cold reservoir temperature, and $\sigma$ is the entropy generation rate. Later, Yan [28] extended it to $E = P - T_0\sigma$, considering the impact of the environment. Furthermore, the ecological function was extended by Chen [29] and it has been widely investigated [30–32]. Hernández et al. [33] proposed the Ω figure of merit, indicating a compromise between energy benefits and losses. By investigating the COP of refrigerators based on the Ω figure of merit, De Tomás et al. [34] and Hernández et al. [35] proposed the upper and lower bounds of COP. Yan and Chen [36] conducted the optimization criterion with the target function $\varepsilon\dot{Q}$, where $\dot{Q}$ is the cooling load rate of the refrigerators. This is the $\chi$ figure of merit for refrigerators. It considers both COP and the cooling rate [21,24,30,37,38]. Taking $\chi$ as the target function in a low dissipation model, Wang et al. [24] proposed that the COP at maximum $\chi$ was bounded between 0 and $(\sqrt{9+8\varepsilon_C}-3)/2$. Under the conditions of symmetric dissipations, the CA coefficient of performance may be retrieved. It has also been obtained in refrigerators with non-isothermal processes [30]. Besides, the $\chi$ criterion has also been adopted to analyze microscopic refrigerators [39,40].

Most of the aforementioned studies on refrigerators have focused on obtaining maximum cooling load rate and maximum COP. However, the objective functions can conflict with each other because maximum cooling load rate sharply decreases COP, whereas maximum COP vanishes the cooling load rate. In the previous literature of the thermally regenerative electrochemical refrigerator system, the time duration of each process has not been considered. The $\chi$ figure of merit considers both the COP and cooling load rate, which can be seen as a compromise between maximum cooling load rate and maximum COP. This criterion could offer an alternative insight into performance analysis for actual thermally regenerative electrochemical refrigerator cycles. In this study, we systematically investigate TRER performance based on the finite time analysis, considering the irreversibility of finite-rate heat transfer and heat leakage. The general expressions of some important parameters of TRER are derived. The impacts of the cell material, heat conductance of heat exchangers, and heat reservoir temperature ratio on the maximum value of $\chi$ criterion and the corresponding cooling load rate and COP are analyzed in detail. Some useful results are drawn that can be helpful for actual application of TRER devices.

## 2. Mathematical model

TREC consists of four processes: heating, charging, cooling, and discharging [15]. The TRER cycle, which is schematically depicted in Fig. 1(a), can be treated as an inversed cycle of the TREC. To clarify the thermodynamic, this cycle is also plotted on a temperature-entropy (T-S) diagram in Fig. 1(b). In process 1–2, the cell is first charged at a higher voltage at $T_L$, and the entropy of the cell increases through heat absorption from the cooled room during the electrochemical reaction. The cell is then heated from $T_L$ to $T_H$ under an open circuit (OC) condition in process 2–3, thus decreasing the open circuit voltage. In process 3–4, the cell is discharged at a lower voltage at $T_H$, and the entropy of the cell decreases through the ejection of heat into the environment. In the final process (4–1), the cell is cooled from $T_H$ to $T_L$ in an open circuit state, thus increasing open circuit voltage. After a cycle, the cell returns to its initial state. The negative temperature coefficient of the cell shifts down the discharging curve at high temperature ($T_H$) below the voltage curve of charging at low temperature ($T_L$). To drive a TRER device, external power (W), which is equal to the difference between charging and discharging energy, should be added as depicted in Fig. 1(c).

The TRER cycle bases on the thermogalvanic effect and temperature dependence of the electrode potential. The isothermal coefficient for the electrode reaction can be defined as [41].

$$\alpha = \left(\frac{\partial E}{\partial T}\right)_{iso}, \tag{1}$$

where $E$ is the electrochemical potential of the electrode reaction. $\alpha$ has opposite signs in charging and discharging processes between the positive and negative electrodes. In a redox electrochemical reaction, an isothermal coefficient for the full cell can be defined when both electrodes are at the same temperature. That is [12].

$$\alpha_c = \left(\frac{\partial E_+}{\partial T}\right)_{iso} - \left(\frac{\partial E_-}{\partial T}\right)_{iso}. \tag{2}$$

In a full cell with an electrode reaction $\Sigma A + ne^- \rightarrow \Sigma B$, the spontaneous reaction in an isothermal process can be written as $\sum \nu_j C_j = 0$, where $C_j$ and $\nu_j$ are the $j$th chemical involved and its stoichiometric number, respectively. $\nu_j$ is positive for A and negative for B. Then the isothermal coefficient can be expressed as

$$\alpha_c = \left(\frac{\partial V_{oc}}{\partial T}\right)_{iso} = \frac{\sum \nu_j s_j}{nF}, \tag{3}$$

where $V_{oc}$ is the open circuit voltage of the full cell in isothermal condition, $s_j$ is the partial molar entropy of the $j$th chemical involved, $n$ is the number of moles of electrons passed per $\nu_j$ mole of $C_j$ reacted, and $F$ is the Faraday constant. In physical chemistry theory, it is well known that the extent of the reaction is equal for all chemicals involved in the reaction, as $\xi = (n_j - n_{j0})/\nu_j$, where $n_{j0}$ is the amount of $j$th chemical at the initial state, and $n_j$ is the amount of $j$th chemical at a certain time during the reaction. Therefore, the entropy change of the charging process at $T_L$ is given by

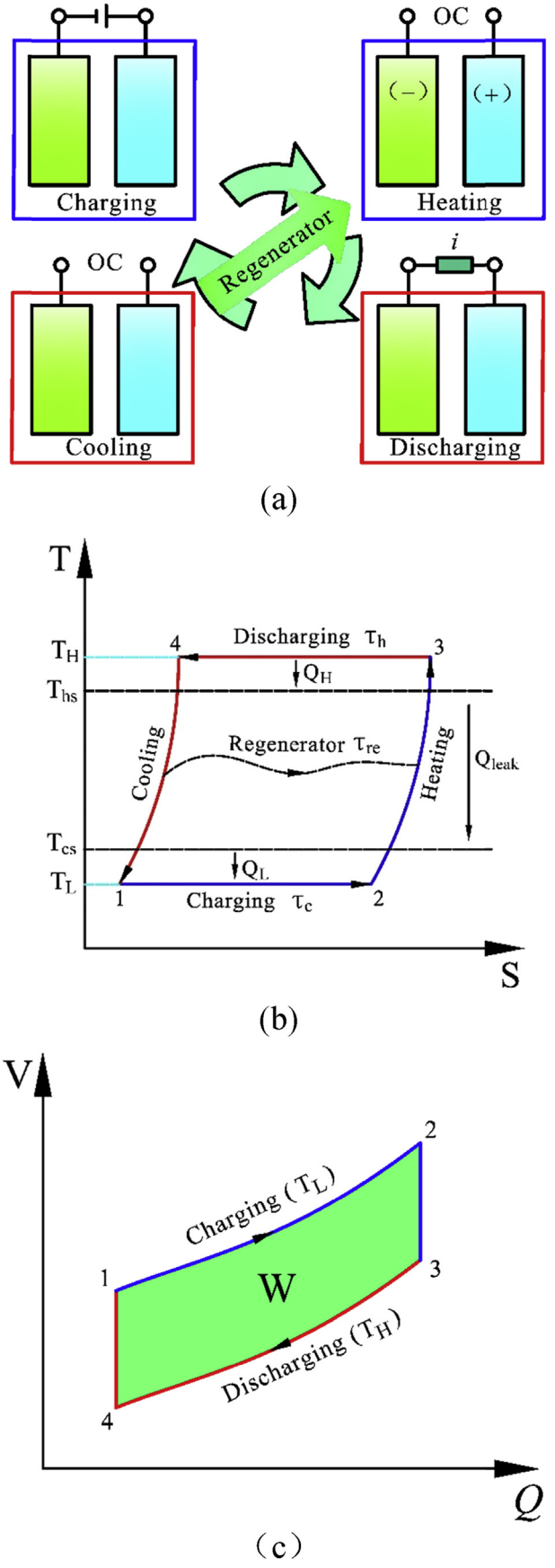


**Fig. 1.** Schematic diagram (a), T-S diagram (b) and voltage-quantity of electric charge (c) for TRER.

$$\Delta S_L = \int_i^f d\xi \sum \nu_j s_j = \int_i^f \alpha_c nF d\xi = \int_i^f \left|\overline{\alpha_c}\right| nF d\xi, \tag{4}$$

where $i$ and $f$ represent the initial ($\Sigma A$) and final ($\Sigma B$) states, respectively.

In order to work as a refrigerator, the cell needs to be charged at $T_L$ and discharged at $T_H$. Because $\alpha_c$ is nearly constant in the range of charging and discharging processes, we can apply the approximation $\overline{\alpha_c} = \alpha_c$, leading to $\Delta S_L = m\alpha_c q_c$, where $m$ is the mass of the cell and $q_c$ is the specific charge capacity, $mq_c$ is the total amount of charge transferred in the charging process at $T_L$. Thus, the heat absorbed from the cooled room during charging process is

$$Q_L = T_L \Delta S_L = m\alpha_c T_L q_c. \tag{5}$$

Similarly, the heat rejected into the environment, denoted by $Q_H$, can be expressed as

$$Q_H = T_H \Delta S_H = m\alpha_c T_H q_c. \tag{6}$$

Furthermore, if we assume that the charging and discharging processes are constant current processes, then the currents are, respectively, given by $I_{ch} = mq_c/\tau_c$ and $I_{dis} = mq_c/\tau_h$, with $\tau_c$ and $\tau_h$ being the durations of the charging and discharging processes. The total energy lost due to the internal resistances during charging and discharging processes is

$$E_{loss} = I_{ch}^2 R_{int} \tau_c + I_{dis}^2 R_{int} \tau_h = m^2 q_c^2 R_{int} (1/\tau_h + 1/\tau_c). \tag{7}$$

Therefore, the energy input in one cycle can be given by

$$W = Q_H - Q_L + E_{loss}. \tag{8}$$

In addition, based on the heat transfer theory, the heat absorbed from cooled space and rejected into the environment can be expressed as

$$Q_L = K_c(T_{cs} - T_L)\tau_c = m\alpha_c T_L q_c, \tag{9}$$

$$Q_H = K_h(T_H - T_{hs})\tau_h = m\alpha_c T_H q_c, \tag{10}$$

where $T_{cs}$ and $T_{hs}$ are the temperatures of cold and hot reservoirs, respectively. $K_c$ and$K_h$ are the heat conductances of cold and hot side heat exchangers, respectively, and are given as $K_c = U_c A_c$ and $K_h = U_h A_h$, where $U_c$ and $U_h$ are the overall heat transfer coefficients, and $A_c$ and $A_h$ are the heat transfer surface areas. According to Eqs. (9) and (10), the time durations of the heat absorption and rejection processes are

$$\tau_c = \frac{m\alpha_c T_L q_c}{K_c(T_{cs} - T_L)}, \tag{11}$$

$$\tau_h = \frac{m\alpha_c T_H q_c}{K_h(T_H - T_{hs})}. \tag{12}$$

The finite heat transfer through the regenerator during the two regenerative processes should also be considered. The regenerative heat loss per cycle, denoted as $\Delta Q_{re}$, is proportional to the temperature difference of the cell as given by Ref. [12].

$$\Delta Q_{re} = mc_p(1 - \eta_{re})(T_H - T_L), \tag{13}$$

where $c_p$ is the specific heat of the cell and $\eta_{re}$ is the effectiveness of the regenerator. In addition, compared to the two isothermal processes, the time required by the regenerative processes is not

negligible. It is assumed to be proportional to the temperature difference of working fluid. Thus [42,43].

$$\tau_{re} = \beta_1(T_H - T_L) + \beta_2(T_H - T_L) = \beta(T_H - T_L), \tag{14}$$

where $\beta_1$ and $\beta_2$ are the proportionality constants in regenerative processes 2–3 and 4–1, respectively. They depend on the property of regenerative material, but are independent of temperature differences. We denote $\beta = \beta_1+\beta_2$. Therefore, the total duration of a cycle can be written as $\tau = \tau_h+\tau_c+\tau_{re}$.

In reality, heat leakage per cycle is usually a proportion between the hot and cold reservoirs, and it is considered by Ref. [44].

$$Q_{leak} = K_l(T_{hs} - T_{cs})\tau, \tag{15}$$

where $K_l$ is the heat leakage coefficient. It is clear that heat leakage does not affect power input. Power input ($P$), cooling load rate ($R$), and COP ($\varepsilon$) are then

$$P = \frac{Q_H - Q_L + E_{loss}}{\tau_h + \tau_c + \tau_{re}}, \tag{16}$$

$$R = \frac{Q_L - \Delta Q_{re} - I_{ch}^2 R_{int}\tau_c - Q_{leak}}{\tau_h + \tau_c + \tau_{re}}, \tag{17}$$

$$\varepsilon = \frac{Q_L - \Delta Q_{re} - I_{ch}^2 R_{int}\tau_c - Q_{leak}}{Q_H - Q_L + E_{loss}}. \tag{18}$$

Based on the aforementioned equations, power input ($P$), cooling load rate ($R$), and COP ($\varepsilon$) of a TRER can be rewritten as

$$P = \frac{\alpha_c(T_H - T_L) + R_{int}\left[\frac{K_c(T_{cs}-T_L)}{\alpha_c T_L} + \frac{K_h(T_H-T_{hs})}{\alpha_c T_H}\right]}{\frac{\alpha_c T_L}{K_c(T_{cs}-T_L)} + \frac{\alpha_c T_H}{K_h(T_H-T_{hs})} + \frac{\beta}{mq_c}(T_H - T_L)} \tag{19}$$

$$R = \frac{\alpha_c T_L - \frac{c_p}{q_c}(1-\eta_{re})(T_H - T_L) - R_{int}\frac{K_c(T_{cs}-T_L)}{\alpha_c T_L}}{\frac{\alpha_c T_L}{K_c(T_{cs}-T_L)} + \frac{\alpha_c T_H}{K_h(T_H-T_{hs})} + \frac{\beta}{mq_c}(T_H - T_L)} - K_l(T_{hs} - T_{cs}) \tag{20}$$

$$\varepsilon = \begin{cases} \dfrac{\alpha_c T_L - \frac{c_p}{q_c}(1-\eta_{re})(T_H - T_L) - R_{int}\frac{K_c(T_{cs}-T_L)}{\alpha_c T_L}}{\alpha_c(T_H - T_L) + R_{int}\left[\frac{K_c(T_{cs}-T_L)}{\alpha_c T_L} + \frac{K_h(T_H-T_{hs})}{\alpha_c T_H}\right]} \\ -K_l(T_{hs} - T_{cs})\dfrac{\frac{\alpha_c T_L}{K_c(T_{cs}-T_L)} + \frac{\alpha_c T_H}{K_h(T_H-T_{hs})} + \frac{\beta}{mq_c}(T_H - T_L)}{\alpha_c(T_H - T_L) + R_{int}\left[\frac{K_c(T_{cs}-T_L)}{\alpha_c T_L} + \frac{K_h(T_H-T_{hs})}{\alpha_c T_H}\right]} \end{cases} \tag{21}$$

Furthermore, the $\chi$ figure of merit, which considers both the cooling rate and COP, can be defined as

$$\chi = R\cdot\varepsilon \tag{22}$$

From Eqs. (19)–(21), a larger internal resistance leads to rapidly increasing power input ($P$), thus decreasing cooling rate ($R$) and COP ($\varepsilon$). Ignoring the effect of internal resistance, for prescribed heat reservoirs and charging and discharging temperatures, a larger isothermal coefficient and specific charging/discharging capacity leads to higher cooling load rate and power input. Better performance of heat exchangers results in less power input and more cooling load rate. The specific heat of the cell and effectiveness of the regenerator have no impact on power input; however, they affect the cooling load rate and COP. Furthermore, a lower heat leakage coefficient contributes to higher cooling rate and COP. However, power input does not vary with increasing or decreasing heat leakage coefficient.

## 3. Optimal operating regions for TRER

For prescribed cell materials and heat reservoirs, it is clearly seen from Eqs. (20)–(22) that the cooling load rate ($R$), COP ($\varepsilon$), and $\chi$ figure of merit are impacted by discharging temperature ($T_H$) and charging temperature ($T_L$). Thus, we can generate the curves of the cooling load rate, COP, and $\chi$ criterion of a TRER versus the ratio of charging and discharging temperature (denoted as $x = T_L/T_H$), as depicted in Fig. 2. With the absence of heat leakage between heat reservoirs, COP increases dramatically with an increasing ratio of charging and discharging temperature ($x$), whereas the cooling load rate and $\chi$ function both exhibit maximum values. When the heat leakage is considered, the curve of COP becomes convex, and also achieves a maximum value. The three maximum values all decrease due to the presence of heat leakage. There exists an optimal charging and discharging temperature ratio that corresponds to the maximum cooling load rate ($R_{max}$ = 146.99 W), maximum COP ($\varepsilon_{max}$ = 2.42), and maximum $\chi$ figure of merit function ($\chi_{max}$ = 209.01 W), which are denoted as $x_{max,R}$ = 0.921, $x_{max,\varepsilon}$ = 0.941, and $x_{max,\chi}$ = 0.933, respectively. Furthermore, we have $x_{max,R}<x_{max,\chi}<x_{max,\varepsilon}$.

We can also obtain the cooling load rate and $\chi$ function versus COP characteristics, as shown in Fig. 3. When heat leakage is absent, the curves of $R-\varepsilon$ and $\chi-\varepsilon$ are convex, whereas the curves become loop-shaped when heat leakage is considered. In addition, the presence of heat leakage reduces the COPs ($\varepsilon_R$ and$\varepsilon_\chi$) that correspond to the maximum cooling rate ($R_{max}$) and maximum $\chi$ figure of merit function ($\chi_{max}$), respectively. For given parameters, we have $\varepsilon_R<\varepsilon_\chi<\varepsilon_{max}$. Fig. 4 illustrates that the $\chi$ figure of merit is also a loop-shaped function of cooling load rate. The curve of $\chi-R$ is always loop-shaped regardless of whether heat leakage is considered. Similarly, the presence of an imperfect regenerator reduces the cooling rate ($R_\chi$) that corresponds to the maximum $\chi$ criterion function ($\chi_{max}$). For given parameters, we have $R_\varepsilon<R_\chi<R_{max}$ and $\chi_\varepsilon<\chi_R<\chi_{max}$.

In general for a refrigerator, it is always preferable to obtain a cooling load rate and COP as large as possible for a given series of

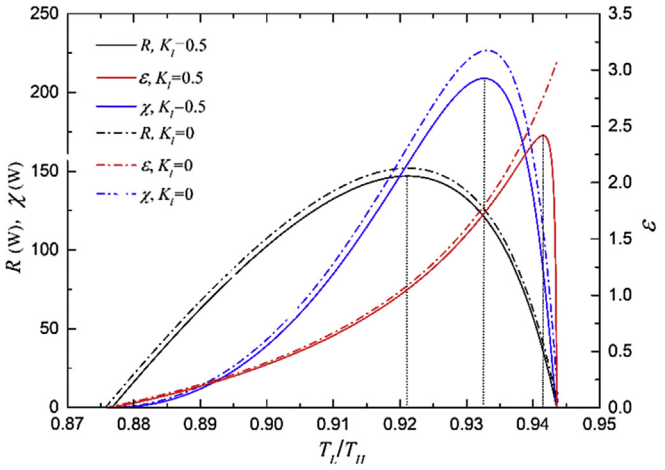


**Fig. 2.** Cooling rate, COP, and $\chi$ figure of merit as functions of charging and discharging temperature ratio for different heat leakage coefficients, where $\alpha_c$ = 0.015 V K$^{-1}$,$q_c$ = 20mA hg$^{-1}$, $c_p$ = 1.5kJ kg$^{-1}$ K$^{-1}$, $R_{int}$ = 0.01 $\Omega$, $m$ = 0.05 kg,$K_h$ = $K_c$ = 70 W K$^{-1}$, $T_{hs}$ = 293.15 K,$T_{cs}$ = 283.15 K,$\beta$ = 0.05 s K$^{-1}$, and $\eta_{re}$ = 0.6.

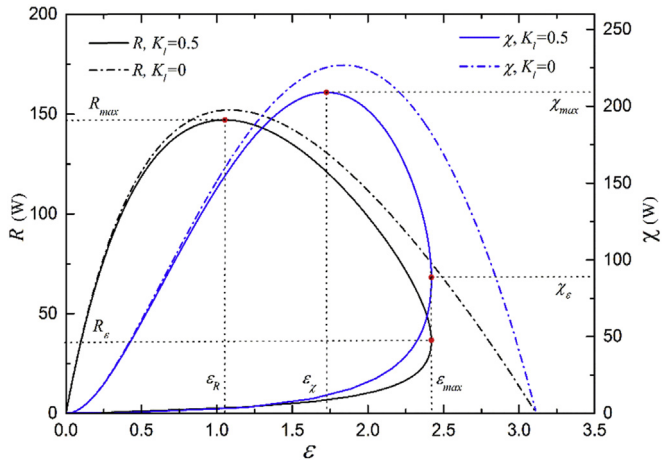


**Fig. 3.** Curves for cooling rate and χ criterion varying with COP for different heat leakage coefficients. Values of given parameters $\alpha_c$, $q_c$, $c_p$, $R_{int}$, $m$, $\beta$, $\eta_{re}$, $K_h$, $K_c$, $T_{hs}$, and $T_{cs}$ are the same as those used in Fig. 2.

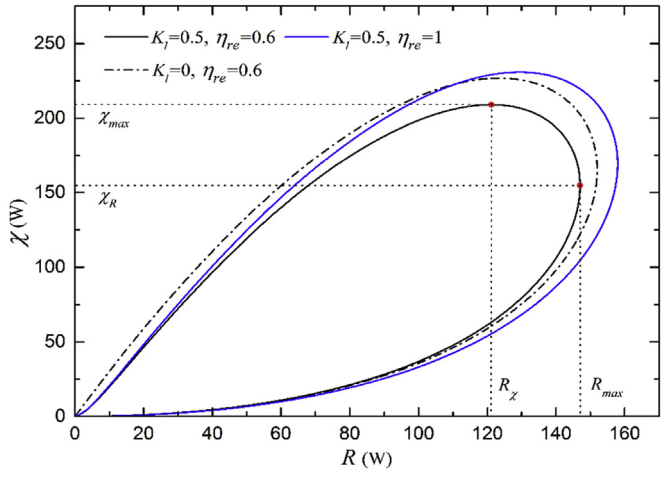


**Fig. 4.** Curves of χ objective function varying with cooling rate for different heat leakage coefficient and effectiveness of regenerator. Values of given parameters $\alpha_c$, $q_c$, $c_p$, $R_{int}$, $m$, $\beta$, $\eta_{re}$, $K_h$, $K_c$, $T_{hs}$, and $T_{cs}$ are the same as those used in Fig. 2.

other parameters. However, according to Figs. 2–4, the larger cooling rate leads to a lower COP, and the larger COP leads to a vanishing cooling load rate. The χ figure of merit is the product of cooling load rate and COP, and thus it considers both as two important parameters (the cooling load rate and COP), which one most concerns. We can trade it as a compromise between the cooling load rate and COP. Therefore, the traditional performance region between maximum cooling rate and maximum COP can be divided into two more specific performance regions (the region between maximum cooling load rate and maximum χ, and the region between maximum χ and maximum COP). These two performance regions represent two different operating demands.

If the main demand is more for cooling load rate, and energy savings is not as important, it is more reasonable for TRER to operate between the performance of maximum cooling load rate and maximum χ figure of merit. In this case, the optimal operating performance of TRER and the ratio of charging and discharging temperature should be situated in

$$R_\chi < R < R_{max}, \quad \varepsilon_R < \varepsilon < \varepsilon_\chi, \quad x_{max,R} < x < x_{max,\chi}. \tag{23}$$

In this region, the cooling load rate decreases with increasing COP, whereas the χ criterion increases with increasing COP and decreases with increasing cooling load rate as depicted in Figs. 3 and 4.

If the main demand is energy savings, but the cooling load rate should also be considered, it is more reasonable for TRER to operate between the performance of the maximum χ criterion and maximum COP. Therefore, the optimal operating performance of TRER and the ratio of charging and discharging temperature should be situated in

$$R_\varepsilon < R < R_\chi, \quad \varepsilon_\chi < \varepsilon < \varepsilon_{max}, \quad x_{max,\chi} < x < x_{max,\varepsilon}. \tag{24}$$

In this region, both the cooling load rate and χ criterion decrease with increasing COP. However, the χ criterion increases with increasing cooling load rate as depicted in Figs. 3 and 4.

## 4. Performance analysis under χ figure of merit

As mentioned above, the χ criterion considers both cooling load rate and COP. Based on the χ figure of merit, the traditional performance region between maximum cooling load rate and maximum COP can be divided into two more specific performance regions. Therefore, the performance of TRER at the χ criterion should be studied.

In order to investigate the optimal performance of TRER at the maximum χ figure of merit, we can maximize the χ objective function with respect to the charging and discharging temperatures, and then optimize it by allowing $\partial\chi/\partial T_H = 0$ and $\partial\chi/\partial T_L = 0$, thus obtaining the maximum value of χ and the corresponding cooling load rate and COP. However, the equations $\partial\chi/\partial T_H = 0$ and $\partial\chi/\partial T_L = 0$ for $T_H$ and $T_L$ are transcendental and cannot be solved analytically. In this section, numerical studies are investigated systematically in order to study the impacts of the cell materials, heat conductance of heat exchangers, and temperature ratio of heat reservoirs on TRER performance under the maximum χ criterion. Here, we set $m = 0.05$ kg, $\beta = 0.05 \mathrm{sK}^{-1}$, $\eta_{re} = 0.6$, and $K_l = 0.5$ W K$^{-1}$.

### 4.1. Impact of cell material

Based on Eqs. (20)–(22), the cell materials that affect the χ criterion performance of TRER are the isothermal coefficient, specific heat, specific charging/discharging capacity, and its internal resistance. Their impacts on the maximum χ figure of merit and its corresponding cooling load rate and COP are depicted in Figs. 5–8 and listed in Table 1. As shown in Fig. 5, the maximum value of χ

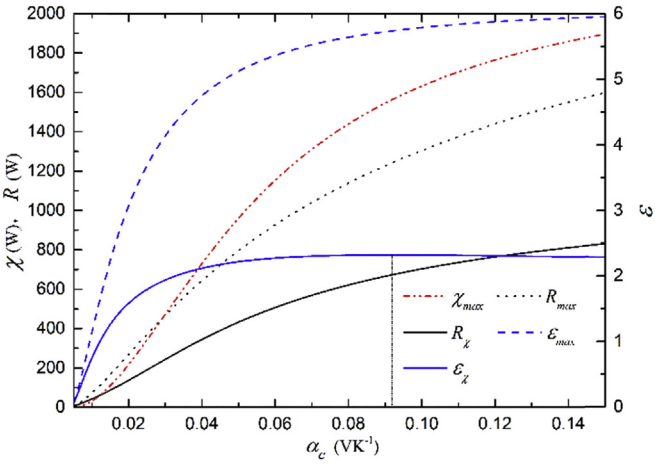


**Fig. 5.** Variation of maximum χ figure of merit function and corresponding cooling load rate and COP with cell isothermal coefficients, where $q_c = 20$ mA hg$^{-1}$, $c_p = 1.5$ kJ kg$^{-1}$ K$^{-1}$, $R_{int} = 0.01$ Ω, $K_h = K_c = 70$ W K$^{-1}$, $T_{hs} = 293.15$ K, and $T_{cs} = 283.15$ K.

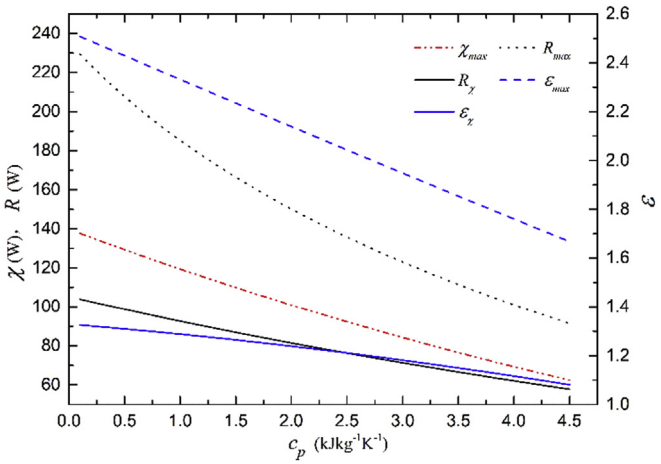


**Fig. 6.** Curves of maximum χ criterion function and corresponding cooling load rate and COP with heat specific, where $\alpha_c = 0.015$ V K$^{-1}$, $q_c = 20$mA hg$^{-1}$,$R_{int} = 0.01$ Ω, $K_h = K_c = 70$ W K$^{-1}$, $T_{hs} = 293.15$ K, and $T_{cs} = 283.15$ K.

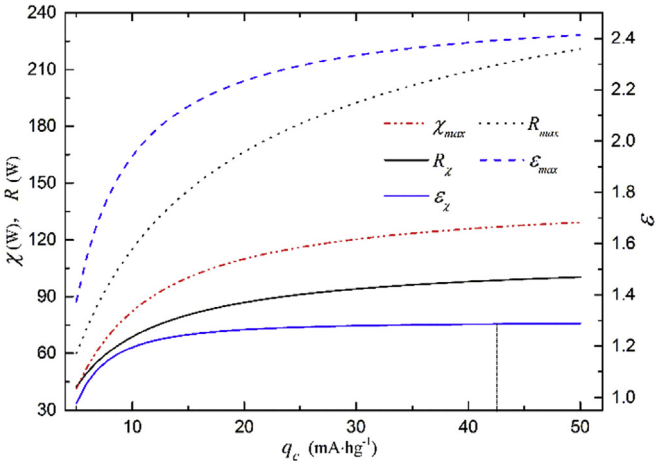


**Fig. 7.** Maximum χ criterion function and corresponding cooling load rate and COP as a function of specific charging/discharging capacity, where $\alpha_c = 0.015$ V K$^{-1}$,$c_p = 1.5$ kJ kg$^{-1}$ K$^{-1}$, $R_{int} = 0.01$ Ω, $K_h = K_c = 70$ W K$^{-1}$, $T_{hs} = 293.15$ K, and $T_{cs} = 283.15$ K.

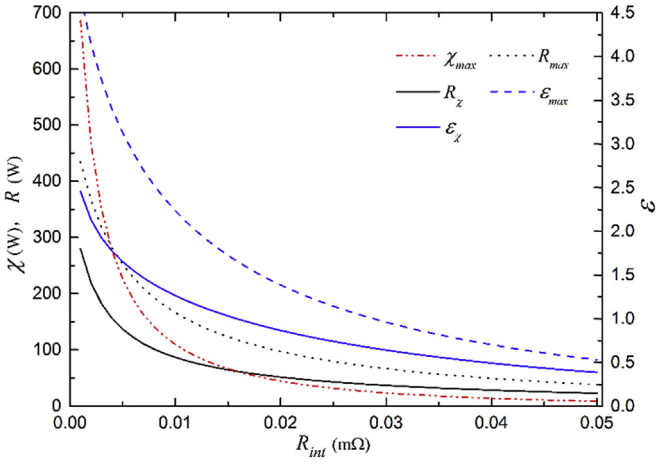


**Fig. 8.** Variation of maximum χ figure of merit and corresponding cooling load rate and COP with internal resistance, where $\alpha_c = 0.015$VK$^{-1}$,$c_p = 1.5$kJ kg$^{-1}$ K$^{-1}$, $q_c = 20$mA hg$^{-1}$, $K_h = K_c = 70$ W K$^{-1}$, $T_{hs} = 293.15$ K, and $T_{cs} = 283.15$ K.

and its corresponding cooling load rate ($R_\chi$) and COP ($\varepsilon_\chi$) increase with increasing isothermal coefficient monotonously. When the isothermal coefficient is smaller than 0.04 V K$^{-1}$, COP at the maximum χ criterion increases rapidly with increasing isothermal coefficient, reaches 44.6–88.3% of the maximum COP. When the isothermal coefficient is larger than 0.04 V K$^{-1}$, COP at the maximum χ criterion exerts a maximum as 2.32 and then decreases slightly, although the maximum χ criterion and its corresponding cooling load rate still increase. There exists an optimal isothermal coefficient as 0.0918 V K$^{-1}$ that leads to a maximum COP under the maximum χ criterion.

Specific heat presents no impact on the power input of TRER; however, it has a significant impact on the value of χ under the maximum χ criterion and its corresponding cooling load rate and COP, which decrease monotonously with increasing specific heat, as depicted in Fig. 6 and Table 1. The impacts of the specific charging/discharging capacity on the maximum χ figure of merit and its corresponding cooling load rate and COP are presented in Fig. 7 and Table 1. When the specific charging/discharging capacity is larger than 41.7 mA hg$^{-1}$, COP at the maximum χ criterion remains stable as 1.286, whereas the maximum χ figure of merit and corresponding cooling load rate still increase, but rather slowly. There also exists a minimum specific charging/discharging capacity as 41.7 mA hg$^{-1}$ that leads to maximum COP at maximum χ criterion condition. Fig. 8 demonstrates that the maximum χ figure of merit and the corresponding cooling load rate and COP all decrease sharply with increasing internal resistance. It can also be clearly seen that the cooling load rate and COP at maximum χ criterion nearly vanish when the internal resistance is larger than 0.05mΩ.

According to the aforementioned analysis, materials with larger isothermal coefficient and specific charging/discharging capacity, lower internal resistance, and specific heat contribute to a better trade-off performance of TRER. The above analysis can serve as a guide for selecting appropriate cell materials for real TRERs.

### 4.2. Impact of heat exchangers

Based on Eqs. (20)–(22), one of characteristics that impact the performance of TRER are the heat conductance of cold and hot side heat exchangers, whose impacts on the cooling load rate and COP under the maximum χ criterion are presented in Figs. 9 and 10. As shown in Fig. 9 and Table 2, in the discharging processes, the maximum χ figure of merit and its corresponding cooling load rate all increase with increasing heat conductance ($K_h$) of the hot side heat exchangers. The corresponding cooling load rate achieves a maximum value as 93.2 W when $K_h = 380$ W K$^{-1}$ and then saturates, whereas the corresponding COP first increases rapidly with increasing heat conductance ($K_h$) of the heat exchangers, achieves a maximum as 1.27 and then decreases, but rather slowly. There exists an optimal value of heat conductance ($K_h$) as 40 W K$^{-1}$ that leads to a maximum COP under the maximum χ criterion condition. In the charging processes, when heat conductance ($K_c$) of the cold side heat exchangers is larger than 180 W K$^{-1}$, the maximum χ figure of merit and its corresponding cooling load rate increase slowly, whereas the corresponding COP achieves a maximum as 1.27 and remains stable.

Therefore, higher performance of the heat exchangers increases the cooling load rate and χ function under the maximum χ figure of merit, but it does not guarantee a higher COP. Furthermore, larger regenerative duration ($\beta$) implies a longer interval in the regenerator, which leads to better heat exchange performance of the regenerator in reality, and thereby increases the cooling load rate and power input. However, it decreases COP. The efficiency of regenerator ($\eta_{re}$) has no impact on power input, but it significantly increases the cooling load rate and COP.

**Table 1**
Performance comparisons under different optimization criterion.

| Parameters of cell materials | Cooling load rate under maximum $\chi$ criterion ($R_\chi$) compared to the maximum cooling load rate criterion ($R_{max}$) | COP under maximum $\chi$ criterion ($\varepsilon_\chi$) compared to maximum COP criterion ($\varepsilon_{max}$) |
|---|---|---|
| Isothermal coefficient $\alpha_c$ | 53.5%–84.8% | 44.6%–88.3% |
| Specific heat $c_p$ | 45.3%–63.2% | 52.8%–64.8% |
| Specific charging/discharging capacity $q_c$ | 45.1%–70.7% | 53.4%–71.1% |
| Internal resistance $R_{int}$ | 52.1%–64.3% | 52.2%–72.9% |

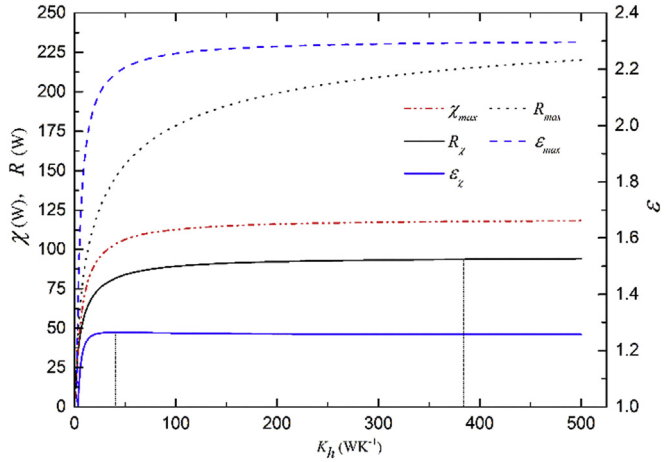


**Fig. 9.** Curves of maximum $\chi$ criterion function and corresponding cooling load rate and COP with respect to heat conductance on hot reservoir side, where $\alpha_c = 0.015$ V K$^{-1}$,$c_p = 1.5$ kJ kg$^{-1}$ K$^{-1}$, $q_c = 20$ mA hg$^{-1}$, $R_{int} = 0.01$ $\Omega$, $K_c = 70$ W K$^{-1}$, $T_{hs} = 293.15$ K, and $T_{cs} = 283.15$ K.

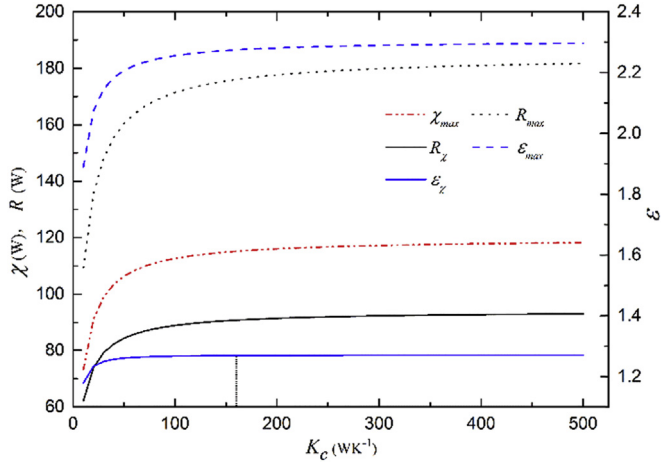


**Fig. 10.** Maximum $\chi$ criterion function and corresponding cooling load rate and COP as a function of heat conductance on cold side heat exchangers, where $\alpha_c = 0.015$ V K$^{-1}$,$c_p = 1.5$kJ kg$^{-1}$ K$^{-1}$, $q_c = 20$ mA hg$^{-1}$,$R_{int} = 0.01$ $\Omega$, $K_c = 70$ W K$^{-1}$, $T_{hs} = 293.15$ K, and $T_{cs} = 283.15$ K.

### 4.3. Impact of temperature ratio of heat reservoirs

The impact of the heat reservoir temperature ratio ($T_{cs}/T_{hs}$) on the maximum $\chi$ criterion function and corresponding cooling load rate and COP is depicted in Fig. 11. It can be seen that the maximum value of $\chi$ and corresponding COP both increase dramatically with increasing temperature ratio of heat reservoirs ($T_{cs}/T_{hs}$). The cooling load rate first increases with increasing temperature ratio, achieves a maximum value as 87.3 W at higher temperature ratio $T_{cs}/T_{hs}$ as 0.91; thereafter, it decreases. There exists an optimal value of heat reservoir temperature ratio that leads to a maximum cooling load rate under the maximum $\chi$ criterion condition.

## 5. Conclusion

The performance analysis and optimization of TRER were investigated based on the finite time analysis with irreversibility of finite-rate heat transfer, regenerative loss, and heat leakage.

The $\chi$ figure of merit considers both COP and cooling load rate. This can be seen as a compromise between maximum cooling load rate and maximum COP. When the heat leakage between the cooling room and environment is considered, COP increases with

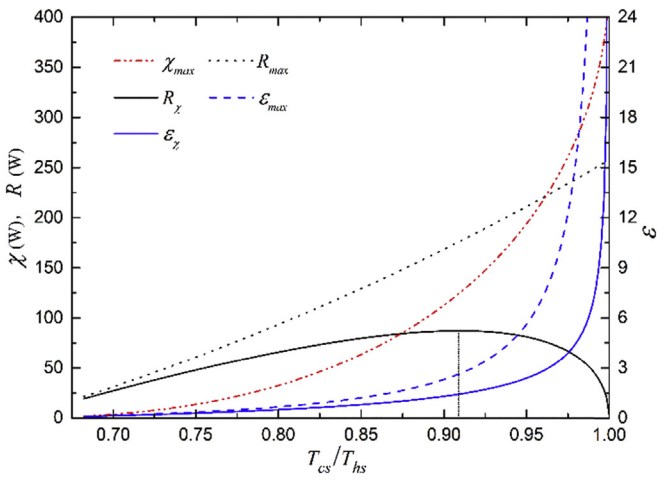


**Fig. 11.** Variation of maximum $\chi$ criterion and corresponding cooling load rate and COP with temperature ratio of heat reservoirs, where $\alpha_c = 0.015$ V K$^{-1}$,$c_p = 1.5$kJ kg$^{-1}$ K$^{-1}$, $q_c = 20$mA hg$^{-1}$,$R_{int} = 0.01\Omega$, and $K_h = K_c = 70$ W K$^{-1}$

**Table 2**
Performance comparisons under different optimization criterion.

| Heat conductance of heat exchangers | Cooling load rate under maximum$\chi$ criterion ($R_\chi$) compared to maximum cooling load rate ($R_{max}$) | COP under the maximum $\chi$ criterion ($\varepsilon_\chi$) compared to the maximum COP ($\varepsilon_{max}$) |
|---|---|---|
| Heat conductance of the hot side heat exchangers $K_h$ | 42.7%–88.5% | 54.8%–87.1% |
| Heat conductance of the cold side heat exchangers $K_c$ | 51.2%–56.8% | 55.3%–62.3% |

increasing $T_L/T_H$ at first, reaches the maximum value, then decreases. The curves of $R-\varepsilon$ and $\chi-\varepsilon$ become closed loop-shaped. However, the curve of $\chi-R$ is always loop-shaped regardless of whether heat leakage is considered. Furthermore, based on the $\chi$ figure of merit, we can divide the performance region between maximum cooling load rate and maximum COP into two more specific performance regions that represent two different operating demands in reality. If the parameters are chosen properly, TRER can be controlled to operate in different optimal regions in order to fulfill the specific demands.

Under the maximum $\chi$ criterion, the impacts of the cell material's characteristics, heat conductance of heat exchangers, and heat reservoir temperature ratio on the corresponding cooling rate and COP were systematically analyzed. For presented heat reservoir temperatures, materials with large isothermal coefficient, and specific charging/discharging capacity, low internal resistance and specific heat lead to higher maximum $\chi$ figure of merit and corresponding cooling load rate and COP. Higher performance of heat exchangers (larger $K_h$ and $K_c$) results in larger maximum $\chi$ function and corresponding cooling load rate, but it does not guarantee a higher corresponding COP. There exists an optimal value of heat reservoir temperature ratio that leads to a maximum cooling load rate under the maximum $\chi$ criterion condition. These results can contribute to more efficient design and operation of TRER devices.

## Acknowledgements

The work was supported by the National Key Basic Research Program of China (973 Program) (2013CB228302).

## Nomenclature

| | |
|---|---|
| $\alpha$ | isothermal coefficients [V $K^{-1}$] |
| $m$ | mass [kg] |
| $Q$ | heat rate [J] |
| $S$ | entropy [J $kg^{-1}$ $K^{-1}$] |
| $T$ | temperature [K] |
| $W$ | work [W] |
| $C_p$ | specific heat [kJ $kg^{-1}$ $K^{-1}$] |
| $E$ | electrochemical potential [V] |
| $E_{loss}$ | energy loss [J] |
| $q_c$ | specific charge capacity [$A\cdot s\cdot kg^{-1}$] |
| $R$ | resistance[$\Omega$] |
| $I$ | currents [A] |
| $\tau$ | time [s] |
| $K$ | heat conductance [W $K^{-1}$] |
| $\beta$ | proportional constant [$s^{-1}$] |
| $\eta_{re}$ | regenerative efficiency |
| $F$ | Faraday constant |
| $\Delta Q_{re}$ | regenerative heat loss [J] |
| $P$ | power [W] |
| $R$ | cooling load rate [W] |
| $\varepsilon$ | coefficient of performance |

*Subscripts*

| | |
|---|---|
| 1, 2, 3, 4 | state point |
| hs | hot reservoir temperature |
| cs | cold reservoir temperature |
| dis | discharging process |
| ch | charging process |
| int | internal |
| H | hot reservoir side |
| L | cold reservoir side |
| re | regenerator |
| l | leakage |

## References

[1] Askalany AA, Salem M, Ismael IM, Ali AHH, Morsy MG, Saha BB. An overview on adsorption pairs for cooling. Renew Sustain Energy Rev 2013;19:565–72.
[2] Ahamed JU, Saidur R, Masjuki HH. A review on exergy analysis of vapor compression refrigeration system. Renew Sustain Energy Rev 2011;15(3):1593–600.
[3] El Fadar A. Thermal behavior and performance assessment of a solar adsorption cooling system with finned adsorber. Energy 2015;83:674–84.
[4] Xi H, Luo L, Fraisse G. Development and applications of solar-based thermoelectric technologies. Renew Sustain Energy Rev 2007;11(5):923–36.
[5] Romero Gómez J, Ferreiro Garcia R, De Miguel Catoira A, Romero Gómez M. Magnetocaloric effect: a review of the thermodynamic cycles in magnetic refrigeration. Renew Sustain Energy Rev 2013;17:74–82.
[6] Gerlach DW, Newell T. An investigation of electrochemical methods for refrigeration. Air Conditioning and Refrigeration Center. College of Engineering. University of Illinois at Urbana-Champaign; 2004.
[7] Long R, Li B, Liu Z, Liu W. Performance analysis of a solar-powered electrochemical refrigerator. Chem Eng J 2016;284:325–32.
[8] Long R, Li B, Liu Z, Liu W. Performance analysis of a solar-powered solid state heat engine for electricity generation. Energy 2015;93:165–72.
[9] Long R, Bao Y, Huang X, Liu W. Exergy analysis and working fluid selection of organic Rankine cycle for low grade waste heat recovery. Energy 2014;73(0):475–83.
[10] Chum HL, Osteryoung RA. Review of thermally regenerative electrochemical systems. 1981. Solar Energy Research Inst., Golden, CO (USA); State Univ. of New York, Buffalo (USA).
[11] Quickenden T, Mua Y. A review of power generation in aqueous thermogalvanic cells. J Electrochem Soc 1995;142(11):3985–94.
[12] Lee SW, Yang Y, Lee HW, Ghasemi H, Kraemer D, Chen G, et al. An electrochemical system for efficiently harvesting low-grade heat energy. Nat Commun 2014;5:3942.
[13] Yang Y, Lee SW, Ghasemi H, Loomis J, Li X, Kraemer D, et al. Charging-free electrochemical system for harvesting low-grade thermal energy. Proc Natl Acad Sci U. S. A 2014;111(48):17011–6.
[14] Yang Y, Loomis J, Ghasemi H, Lee SW, Wang YJ, Cui Y, et al. Membrane-free battery for harvesting low-grade thermal energy. Nano Lett 2014;14(11):6578–83.
[15] Long R, Li B, Liu Z, Liu W. Performance analysis of a thermally regenerative electrochemical cycle for harvesting waste heat. Energy 2015;87:463–9.
[16] Long R, Li B, Liu Z, Liu W. Multi-objective optimization of a continuous thermally regenerative electrochemical cycle for waste heat recovery. Energy 2015;93:1022–9.
[17] Long R, Li B, Liu Z, Liu W. A hybrid system using a regenerative electrochemical cycle to harvest waste heat from the proton exchange membrane fuel cell. Energy 2015;93:2079–86.
[18] Chen Co-K, Su Y-F. Exergetic efficiency optimization for an irreversible Brayton refrigeration cycle. Int J Therm Sci 2005;44(3):303–10.
[19] Chen L, Zhang W, Sun F. Power, efficiency, entropy-generation rate and ecological optimization for a class of generalized irreversible universal heat-engine cycles. Appl Energy 2007;84(5):512–25.
[20] Long R, Liu Z, Liu W. Performance optimization of minimally nonlinear irreversible heat engines and refrigerators under a trade-off figure of merit. Phys Rev E 2014;89(6):062119.
[21] Long R, Liu W. Coefficient of performance and its bounds with the figure of merit for a general refrigerator. Phys Scr 2015;90(2):025207.
[22] Chen L, Wu C, Sun F. Finite time thermodynamic optimization or entropy generation minimization of energy systems. J Non Equilibrium Thermodyn 1999;24(4):327–59.
[23] Li J, Chen L, Ge Y, Sun F. Progress in the study on finite time thermodynamic optimization for direct and reverse two-heat-reservoir thermodynamic cycles. Acta Phys Sin 2013;62(13):130501.
[24] Wang Y, Li M, Tu ZC, Hernández AC, Roco JMM. Coefficient of performance at maximum figure of merit and its bounds for low-dissipation Carnot-like refrigerators. Phys Rev E 2012;86(1):011127.
[25] Velasco S, Roco JMM, Medina A, Hernández AC. New performance bounds for a finite-time Carnot refrigerator. Phys Rev Lett 1997;78(17):3241–4.
[26] Jiménez de Cisneros B, Arias-Hernández LA, Hernández AC. Linear irreversible thermodynamics and coefficient of performance. Phys Rev E 2006;73(5):057103.
[27] Angulo-Brown F. An ecological optimization criterion for finite-time heat engines. J Appl Phys 1991;69(11):7465–9.
[28] Yan Z. Comment on "An ecological optimization criterion for finite-time heat engines" [J. Appl. Phys. 69, 7465 (1991)]. J Appl Phys 1993;73(7):3583.
[29] Zhou J, Chen L, Sun F, Wu C. Ecological optimization for generalized irreversible carnot engines. Appl Energy 2004;77(3):327–38.
[30] Long R, Liu W. Coefficient of performance and its bounds for general refrigerators with nonisothermal processes. J Phys A Math Theor 2014;47(32):325002.
[31] Long R, Liu W. Ecological optimization for general heat engines. Phys A Stat Mech Appl 2015;434:232–9.
[32] Wu X, Chen L, Ge Y, Sun F. Local stability of a non-endoreversible Carnot refrigerator working at the maximum ecological function. Appl Math Model 2015;39(5–6):1689–700.

[33] Hernández AC, Medina A, Roco JM, White JA, Velasco S. Unified optimization criterion for energy converters. Phys Rev E Stat Nonlinear Soft Matter Phys 2001;63:037102.
[34] De Tomás C, Roco JMM, Hernández AC, Wang Y, Tu ZC. Low-dissipation heat devices: unified trade-off optimization and bounds. Phys Rev E 2013;87(1):012105.
[35] Hu Y, Wu F, Ma Y, He J, Wang J, Hernández AC, et al. Coefficient of performance for a low-dissipation Carnot-like refrigerator with nonadiabatic dissipation. Phys Rev E Stat Nonlinear Soft Matter Phys 2013;88(6):062115.
[36] Yan Z, Chen J. A class of irreversible Carnot refrigeration cycles with a general heat transfer law. J Phys D Appl Phys 1990;(2):136–41.
[37] Long R, Liu W. Unified trade-off optimization for general heat devices with nonisothermal processes. Phys Rev E 2015;91(4):042127.
[38] De Tomás C, Hernández AC, Roco JMM. Optimal low symmetric dissipation Carnot engines and refrigerators. Phys Rev E 2012;85(1):010104.
[39] Long R, Liu W. Performance of quantum Otto refrigerators with squeezing. Phys Rev E 2015;91(6):062137.
[40] Long R, Liu W. Performance of micro two-level heat devices with prior information. Phys Lett A 2015;379(36):1979–82.
[41] DeBethune A, Licht T, Swendeman N. The temperature coefficients of electrode potentials the isothermal and thermal coefficients—The standard ionic entropy of electrochemical transport of the hydrogen ion. J Electrochem Soc 1959;106(7):616–25.
[42] Wu F, Chen L, Wu C, Sun F. Optimum performance of irreversible Stirling engine with imperfect regeneration. Energy Convers Manag 1998;39(8):727–32.
[43] Kaushik SC, Kumar S. Finite time thermodynamic analysis of endoreversible Stirling heat engine with regenerative losses. Energy 2000;25(10):989–1003.
[44] Chen L, Feng H, Sun F. Optimal piston speed ratio analyses for irreversible Carnot refrigerator and heat pump using finite time thermodynamics, finite speed thermodynamics and direct method. J Energy Inst 2011;84(2):105–12.